Monte Carlo simulations of hyper-velocity particulate mechanics within silicon micropore optics

Conference or Workshop Item

Monte Carlo simulations of hyper-velocity particulate mechanics within silicon micropore optics

T W Buggey[a], M R Soman[a], J Keelan[a], D J Hall[a], A D Holland[a].

[a] Centre for Electronic Imaging (CEI), The Open University, Milton Keynes, UK

ABSTRACT

The focal planes of X-ray astronomy missions are at risk of particulate impacts from both micrometeoroids and orbital debris due to the open aperture of the narrow-angle incidence optics. Silicon micro-pore optics (sMPOs) have seen significant development due to their wide-angle observing capabilities and are planned for use in future X-ray space missions such as SMILE and THESEUS. Although previous space missions have seen sporadic and disruptive events in detectors which are attributed to particulate impacts, the number of particulates that can traverse the new sMPO and affect detector performance is not currently known, preventing the quantification of damage on focal planes.

Work carried out on nested shell X-ray optics suggested that hyper-velocity particulates could scatter from the polished inner-mirrors and be focused on the focal plane of an instrument. By assuming that this basic scattering mechanic is present in sMPO, along with the natural clear path from space to the focal plane, the overall transmission rate of particulates through such an optic can be calculated using the Monte Carlo simulation methodology.

By using the simulation presented here, along with known micrometeoroid flux models and so-called damage equations, the risk to focal planes of large-scale space missions due to hyper-velocity particulate impacts can for the first time be quantified. As such, the work presented here has many applications and uses across a wide range of fields.

Keywords: micrometeoroid, orbital debris, Monte Carlo, silicon micropore optics, impact, space missions.

1 Introduction

Space-based, soft X-ray detectors have been utilised for many decades to observe a myriad of soft X-ray sources including gamma-ray bursts, neutron stars as well as many other hot astronomical objects [1,2]. Although observing from space removes the problem of atmospheric absorption, it does however, come with downsides such as a harsh environment in the form of radiation and hyper-velocity particulates. The effect of the space radiation environment has been studied extensively, with every component on a space-based X-ray telescope undergoing significant testing and adaptation for radiation hardness. This includes crucial components such as detectors, electronics, and sensitive materials. The effect of hyper-velocity particulate impacts has had significantly less research, partly due to the sporadic nature of hyper-velocity particulates, while also partly due to less overall risk as the majority of key components are physically shielded by the spacecraft itself. The main risk from hyper-velocity particulates is from parts of the spacecraft that are directly open to space, most notably in this study the mission-critical detectors.

Modern advances in soft X-ray optics, such as the development of silicon micro-pore optics (sMPO) provide significant advances in field of view while offering reduced mass for the same performance [3]. Downsides also come however, as sMPO provide direct line of sight from space to the sensitive X-ray detectors, increasing the risk of a potentially fatal hyper-velocity particulate impact. Future soft X-ray telescopes must consider the risk of particulate impacts, which will require new insight into the interaction of particulates with the optics themselves as well as knowing the direct effect of particulate impacts on the detectors themselves.

To fully understand the risk and effects to the detectors and optics from particulate impacts, questions require answering such as:

- What are the mechanisms that control the passage of particulates through sMPO?
- Once understood, how many particulates are able to pass through the optics and hence impact the focal plane?

To answer these questions, simulations are required which accurately replicate the physical mechanisms present in sMPO and can calculate the transmission rate of hyper-velocity particulates.

2 Silicon Micropore Optics

Future soft X-ray space missions will potentially utilise the next generation of X-ray optics, silicon micropore optics (sMPO). Significant effort has been put into the development of this new type of optic, as it offers a wider field of view and improved energy resolution, while having a lower mass budget compared to that of previous X-ray optics (nested mirrors) [3]. The new optical system is comprised of many small micropores with highly polished interiors, allowing narrow-angle deflection of soft X-rays. The optics are often assembled on a slumped surface, such that the pores all focus on the focal plane of the instrument in question. Figure 1 shows a sMPO system integrated into the Soft X-ray Imager as part of the European Space Agency SMILE SXI mission.

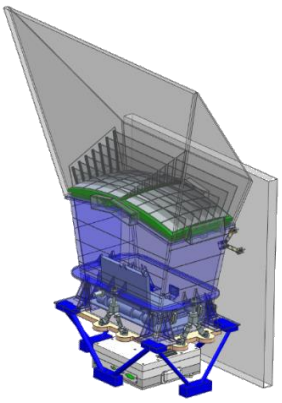

Figure 1: SXI instrument with the sMPO modules assembled within the large green squares [8].

Figure 2 (left) shows an image of a grid of micropores and Figure 2 (right) shows a schematic of four micropores with labelled dimensions. The opening of each pore dictates the active area of the optics, which is defined by the area available for photons to enter the entire optical system. Ideally the width of the walls between each micropore is minimal, to be able to maximise the active area, but manufacturing constraints place minimum limits on the wall widths.

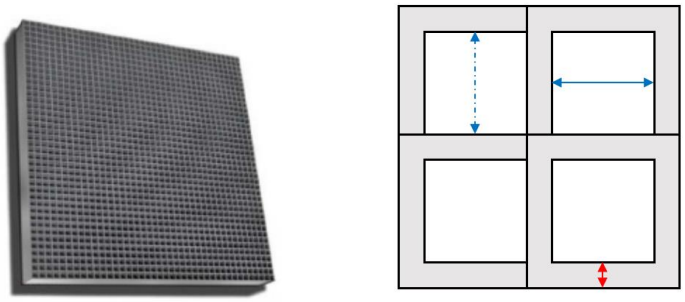

Figure 2: Left – A grid of micropores, similar to one module seen in Figure 1[9]. Right – Schematic of four example micropores. The grey area shows the spacers between each pore (red arrow) and is equidistant for all micropores within manufacturing constraints. The white area represents the “open” area of the pores, with pore widths and lengths given by the bold blue and dashed lines respectively.

2.1 Defining the pore ratio

Silicon micropore dimensions can be defined by a specific pore ratio (R), which is the ratio of the width (or length) to the depth of the pore (shown in Figure 3). Silicon micropores generally have square openings (equal width to length) and have R values of >20, to maximise the internal scattering surface for soft X-ray photons.

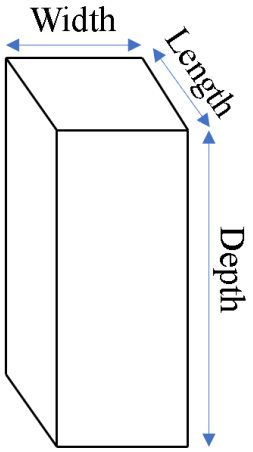

Figure 3: Schematic of a silicon micropore with labelled dimensions. The depth of micropores are often significantly longer than the pore opening diameter, although this can vary dependant on the application.

3 Previous studies

The foundation of the original work presented here will utilise phenomena found in peer reviewed work. Most notably, previous work looking at the mechanics of particulate scattering in soft X-ray optics will be discussed.

3.1 Particulate scattering in soft X-ray optics

Previous authors (Abbey et al. 2006 [5]; Meidinger et al. 2003 [4]; Palmieri 2004 [6]) have shown that a scattering mechanism exists in nested X-ray mirrors whereby incident particulates are deflected after collision with the polished inner mirror surface. The specific scattering mechanism occurs for particulate angles of **at least 5°**, although no upper limit is currently known. An upper limit can be inferred via in-orbit data in the case of Abbey et al. (2006) [5], by taking the number of known impacts over a case study (XMM-Newton in this case). An upper limit to the acceptance angle was found to be **~8°** in this case.

However, a number of future soft X-ray space telescopes, as stated earlier, will use the next generation of soft X-ray optic as opposed to Wolter-type technology. Parallels can still be drawn without thorough analysis however, as the radius of curvature across is often low for sMPO (~mm), meaning that particulates will be incident upon an approximately flat and polished surface, very similar to the nested mirror geometry. Therefore, for the remainder of the analysis presented here, the same scattering behaviour will be assumed although it has not been proven explicitly.

If it is assumed that scattering does exist, the specific scattering angles will need to be clearly defined to produce a reasonable simulation. However, no experimental studies exist so far, therefore it will be assumed that particulates incident with **angles under 5°** will scatter from the polished inner surfaces of the sMPO.

4 Monte Carlo simulations

The simulation proposed has several stages to accurately represent the total particulate flux that traverses a micropore. A qualitative description is given below of each stage:

1. Generate initial particulate coordinates in spherical coordinates considering the cosine distribution for angular particulate distributions [7].
2. Generate secondary particulate coordinates on an area equal to the dimensions of the open area of a micropore.
3. Using both sets of coordinates, trace the trajectories of each particulate through a distance equal to the depth of one micropore.
4. Take the final coordinates and calculate the number of particulates that exit an area which aligns with the exit to the simulated micropore, while also incorporating particulate diameter.
5. For the particulates that do not fall into the designate area, using trigonometry to calculate the angle in which each particulate strikes the inner wall of the micropore.
6. The final transmission rate is equal to the ratio of incident particulates over the sum of the particulates which exit the micropore directly and the particulates which strike the inner walls with an angle of < critical angle of deflection.

4.1 Coordinate system

Before running the simulation, the coordinate geometry must be generated correctly to ensure a physical simulation. Figure 4 shows a reconstructed cubic structure representing a micropore of 4x4x4 units. The centre of the pore aligns with (0,0) in the XY plane, indicated by the black dashed line. The entrance to the pore is represented by a 4x4 square mesh grid, in the Z = 0 plane. The exit of the pore is located in identical XY coordinates, but with a Z coordinated below 0, in the case of Figure 4 the identical 4x4 mesh grid is located in the plane Z = -4. The azimuth coordinate is defined as the plane between dashed red and blue line rotated around the black dashed line. The elevation angle is defined as the angle measured between the red dashed line and the black dashed line. Finally, the radial component is defined as the distance of the vector originating from (0,0,0).

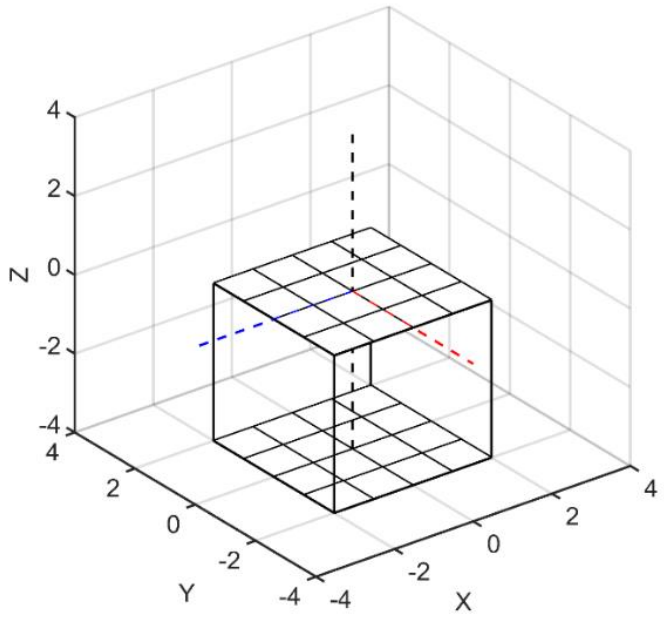

Figure 4: Representation of a single micropore. Additional vectors connecting the entrance mesh and exit mesh have been shown for clarity although they do not affect the result of the simulation. Arbitrary units are also used as the only key dimension in the simulation is the R ratio.

4.2 Generating initial coordinates

For initial particulate coordinate generation, spherical polar coordinates are used as this geometry is more suitable for the angular cosine distribution. Once generated, the spherical polar coordinates can be translated into cartesian coordinates for the ray tracing part of the simulation. Figure 5 shows the initial distributions of particulate coordinates in both spherical polar and cartesian coordinates.

Particulate coordinates in the azimuth and elevation direction are generated by a pseudo-random number generator. The azimuth direction is scaled between 0 – 360 degrees as particulates can strike the optics from any direction, show by a flat distribution in Figure 5 (top-left). The elevation angle is scaled between 0 – 90 degrees to ensure particulates can only strike one side of the optics (0 – 180 degrees) and also to avoid double counting when using an azimuth angle between 0 – 360 degrees. The flat elevation angle is then scaled by a cosine distribution, which appears as a sine distribution as generally the cosine distribution angle is measured by the normal to the surface (the plan of the micropore entrance in this case). The radial direction is taken as constant as this does not affect the results of the simulation.

Spherical polar coordinates are then converted to cartesian and are shown in the lower half of Figure 5. Both X and Y coordinates show a weighting towards 0 respectively. A coordinate of (0,0) represents the centre of a square micropore (also seen in Figure 4), meaning that initial particulate coordinates are preferentially directly above the centre of the pore (as expected).

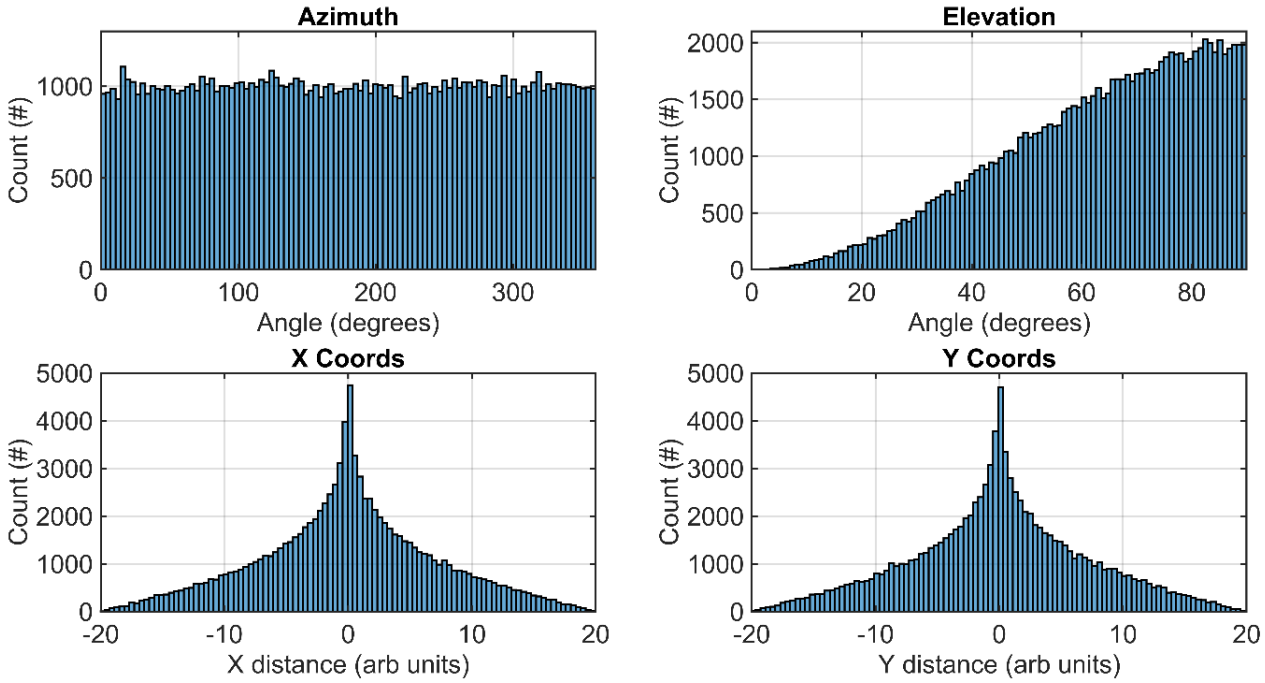

Figure 5: Distributions of initial particulate coordinates in both cartesian and spherical polar coordinates.

4.3 Pore entrance distributions and ray tracing

Once initial spherical polar coordinates are generated and transformed to cartesian coordinates, the next stage is to generate entrance coordinates where particulates will enter the open micropore area. Figure 6 (left) shows the random distribution of points in X and Y in a 4x4 grid. Once micropore entrance coordinates are generated, the initial coordinates can be connected to the micropore entrance coordinates to create particulate tracks as seen by the blue lines in Figure 6 (right).

After the tracks are created, the vectors can be extruded following the same trajectory until the designated Z plane is reached (Z = - 4 in this case), as seen by the red lines in Figure 6 (right). The depth of extrusion represents the depth of a micropore, specific to that simulation of a given R ratio. Once extrusion is complete, the combination of each blue and

red track represents a particulate trajectory originating from space, entering the pore at random locations and either exiting the micropore at an equivalent depth or colliding with an inner polished surface.

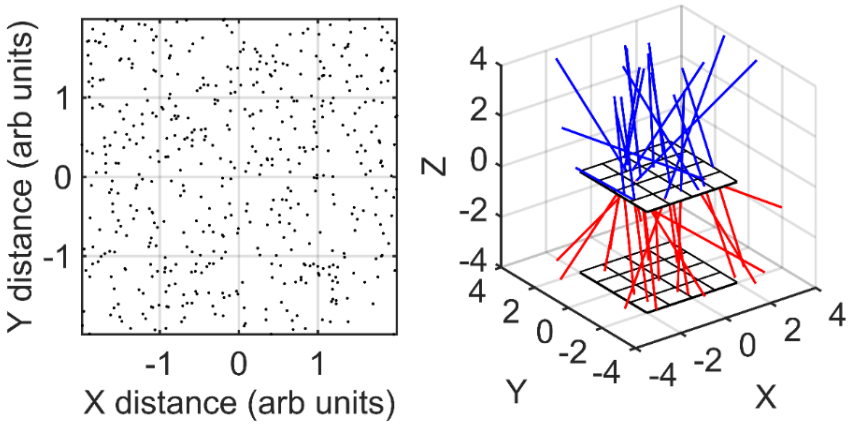

Figure 6: Left – Distribution of particulate entry points over a single micropore. Right - 3D representation of full particulate tracks through an example micropore of dimensions 4x4x4 arbitrary units. Note that the number of points and tracks on the right-hand plot is significantly less than the left-hand plot for clarity. The pore depth chosen is also unrealistic, as most micropores are significantly longer than the entry dimensions. The cubic pore dimensions were only chosen for illustrative purposes.

4.4 Pore entrance and exit distributions for differing pore ratios

Once ray tracing is complete, the entry and exit coordinates of each particulate can be interrogated for the necessary information regarding direct, non-direct or no transmission. Before this stage however, it is necessary to check the coordinate distributions to ensure they are as expected. Figure 7 shows the distributions of both entrance and exit coordinates for four different sizes of micropores. Each micropore is described by the R value, a high R value suggests a long and thin micropore, whereas an R value of 1 represents a cubic micropore. By looking at the entry and exit coordinates relative to the pore ratio, it is possible to check whether the simulation is producing physical and expected results.

Figure 7 (top-right) shows the distributions of entry and exit points for the four different micropore dimensions, with the X and Y dimensions matching those seen in Figure 4 and Figure 6. The micropore entry coordinates (black dots) show a sharp square distribution also seen in the XY histograms. This is as expected as any black dot outside the ranges between -2 and 2 in both X and Y would suggest that the incident particulate has not entered the micropore. The distribution is also relatively flat in X and Y due to the random nature of the generation of particulate entry point, which is also as expected.

The remaining coloured points represent exit coordinates for differing pore ratios. As the pore ratio is decreased from 30 to 1, the distribution of exit coordinates changes, with a higher number of points distributed around the 2x2 grid, seen most clearly via the pink dots. This suggests that for longer pores (with a higher R), particulates are spreading over a wider XY range when reaching the designated Z plane, which is physically expected and intuitive.

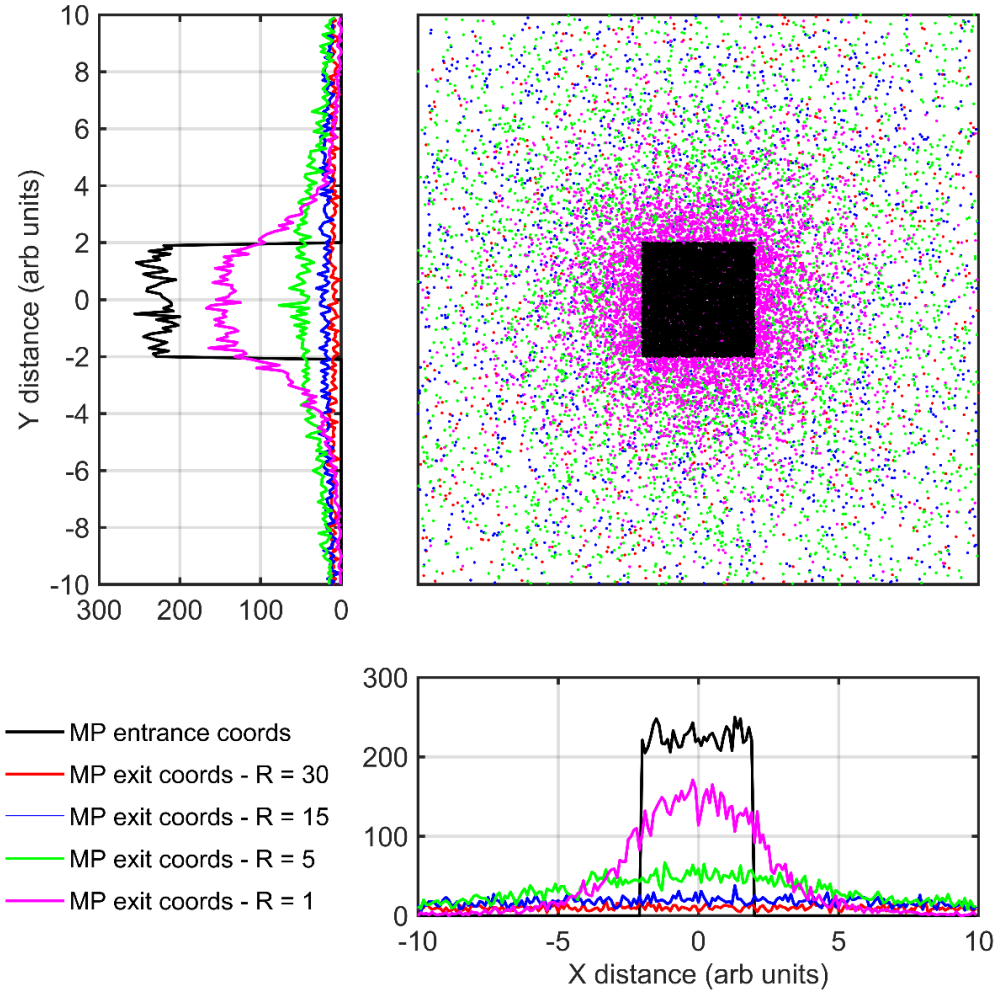

Figure 7: Spatial distributions of both entry and exit coordinates for different simulated micropore ratios. Note that only the black points represent entrance coordinates, as the generation of entrance coordinates is independent of micropore ratio.

4.5 Incorporating particulate diameter

The analysis until this stage has assumed that the simulated particulates are point sources and can be modelled as such. However, physically, each particulate has a set diameter that will alter the mechanics of interactions with the micropore. The main effect of particulate diameter is to reduce the effective open area of each micropore, by an amount proportional to the diameter of the incident particulate.

Figure 8 (left) shows a schematic of a birds-eye view of the entrance to a 4x4 unit micropore centred on the origin (0,0). The micropore has a width and length defined by the solid black line. Also shown are four particulates in black, pink, blue and red with different coordinates, indicating the XY coordinate in which they potentially enter the micropore. The pink and black particulate have an entrance coordinate such that the particulate collides with the edge of the micropore (given the particulate diameter). It is assumed that if this occurs, the particulate cannot enter the micropore and thus cannot be transmitted (0% chance of transmission through the micropore). On the other hand, the red and blue particulate have coordinates which means that the particulate does not collide with the spacers between the pores and can successfully enter the micropore.

To quantify this effect, the pore area can be reduced, leading to an “effective” pore area (EPA, indicated by black dashed line in Figure 8 – left), based upon the radius of the particulate. To validate this stage of the simulation, the effective pore

area can be plotted vs particulate diameter for different sizes of pores, as seen in Figure 8 (right). As expected, the effective area of each pore decreases as particulate diameter increases. For smaller pore sizes, the effective area decreases at a faster rate, as each particulate diameter takes up a larger proportion of the initial micropore size. The effective pore area for each pore size also reduces to zero as soon as the particulate diameter is equal to the size of the pore. Physically, this makes sense as the micropore opening is not large enough for the particulate to enter the micropore.

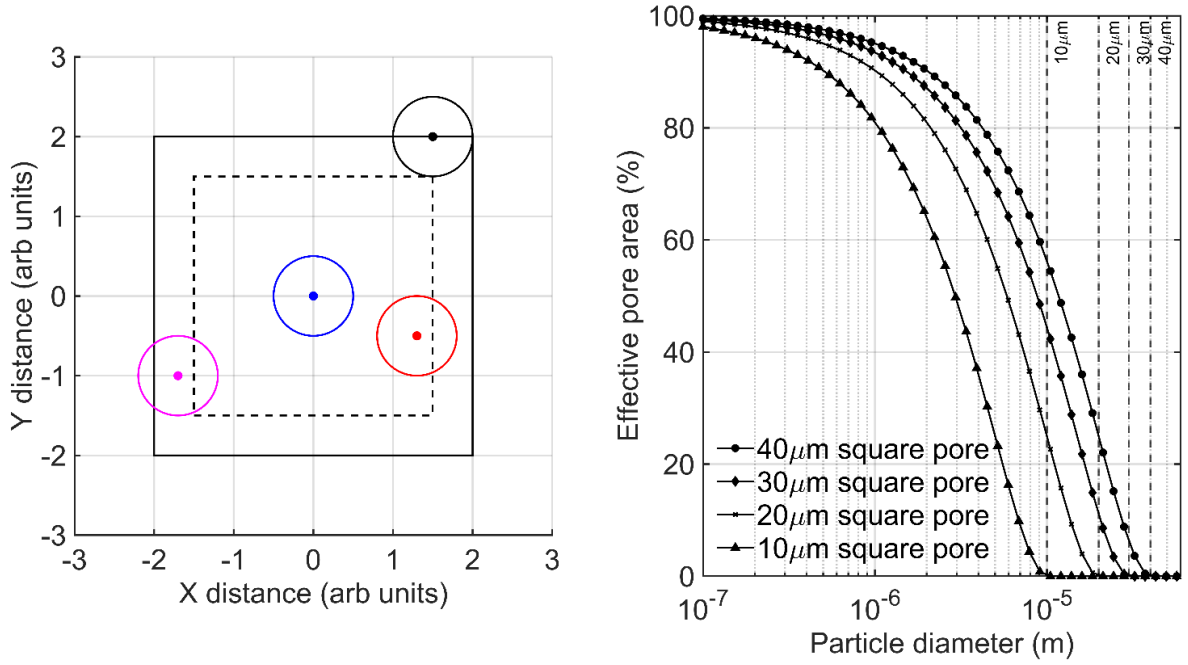

Figure 8: Effect of particulate diameter on pore area. Left – Schematic illustrating the change in effective pore area due to particulate diameter for four different particulate entrance coordinates. Right – Variation in effective pore area for different size pores.

4.6 Calculating particulate transmission rates

Once ray tracing is complete, the number of particulates that traverse a single micropore can be calculated. The total transmission rate is given by the following equation:

$$\text{Transmission rate} = \frac{N_{P_d} + N_{P_n}}{N_{P_t}} \qquad \text{Eq. 1}$$

where:

- N_{Pd} is the total number of particulates that are transmitted directly through the micropore
- N_{Pn} is the total number of particulates that are transmitted indirectly through the micropore
- N_{Pt} is the total number of particulates incident on the micropore

The following section will outline explicitly how the simulation calculates the number of particulates that are both directly and non-directly transmitted through a single micropore.

4.7 Calculating the number of directly transmitted particulates

A particulate that is transmitted directly through a single micropore is defined as a particulate that traverses a single micropore without scattering from an inner pore surface. For a particulate track to be classified as a directly transmitted particulate, it must meet two simple criteria:

- The XY coordinate of the particulate track entering the micropore must fall within the effective pore area.
- The XY coordinate of the particulate track exiting the micropore must fall within the effective pore area.

Figure 9 illustrates the selection process for five particulate tracks, showing both the XY coordinates for the entrance and exit from the micropore, along with the particulate tracks themselves. In the example of Figure 9 (left), a birds eye view of the entrance (grey square) and EPA due to particulate size are shown (black square). Each point with a dashed outline represents the entrance coordinate, with the solid outline of the same colour representing the exit coordinate of the same particulate. To complement, the 3D tracks of the same five particulate tracks are shown in the right half of Figure 9 for clarity. In the example below, the black, blue and red particulate would successfully traverse the micropore and be included in the total number of directly transmitted particulates. The green and pink particulate, however, do not meet the two requirements above, so will need further analysis to determine whether the particulate is treated as a non-directly transmitted particulate.

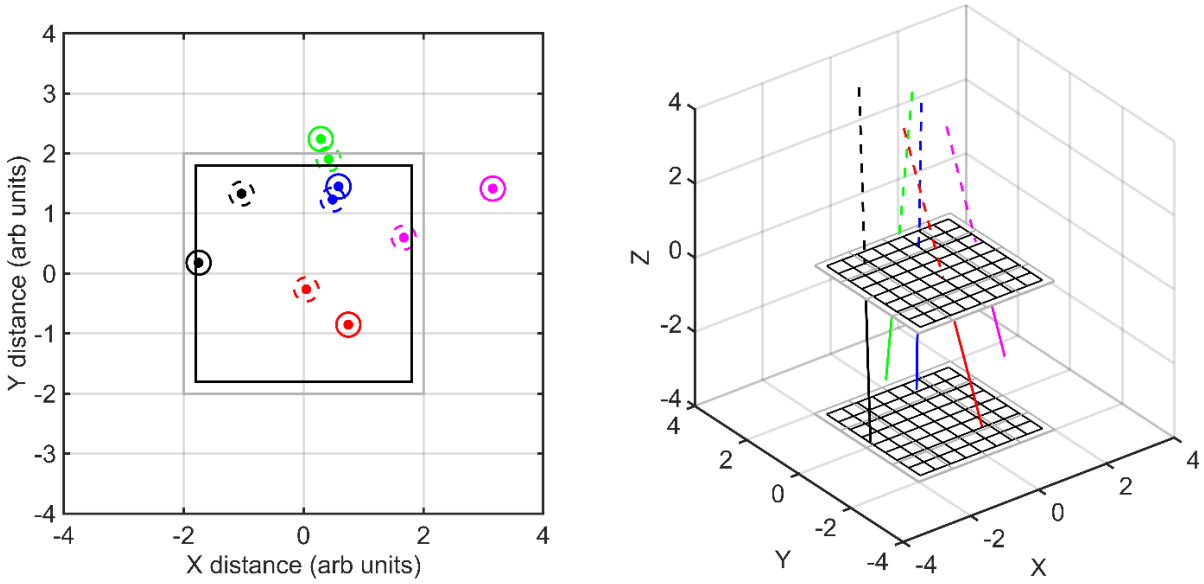

Figure 9: Illustration of the down-selection process of particulate tracks. Left – Birds eye view of the micropore entrance and exit. Right – Complete particulate tracks showing expected trajectories in relation to the entrance and exit of a micropore. The colour of each track is coordinated with the same points in the left section of the figure.

4.8 Calculating the number of non-directly transmitted particulates

A non-directly transmitted particulate is defined as a particulate (or particulate track) that successfully traverses a single micropore by scattering off the inner polished walls. For a particulate to be considered a non-directly transmitted particulate it must therefore meet two criteria:

- The XY coordinate of the particulate track entering the micropore must fall within the effective pore area.
- The incident angle of the particulate track must be less than or equal to the critical scattering angle.

The first criteria is calculated in the same was as directly transmitted particulates. The second criteria, however, requires use of the known particulate coordinates, along with basic geometry and subsequent calculations. Figure 10 shows the particulate track geometry, (red), associated micropore (blue) and the three coordinates used in the simulation. P_1 represents the initial particulate coordinates, P_2 and P_3 represents the XY coordinates in the Z plane of the micropore entrance and exit, respectively.

The incident angle is shown as angle a in Figure 10 (left), and calculation of this angle via trigonometry would require additional knowledge of the coordinate where the particulate strikes the wall of the simulated micropore. However, due to geometry, angle b is equal to a, and is given by the equation:

$$\tan(b) = \frac{q}{z} \qquad \text{Eq. 2}$$

To calculate distance q, Pythagoras' theorem is used, by utilising knowledge of the coordinates already known (shown by Figure *10* – right):

$$q = \sqrt{x^2 + y^2} \qquad \text{Eq. 3}$$

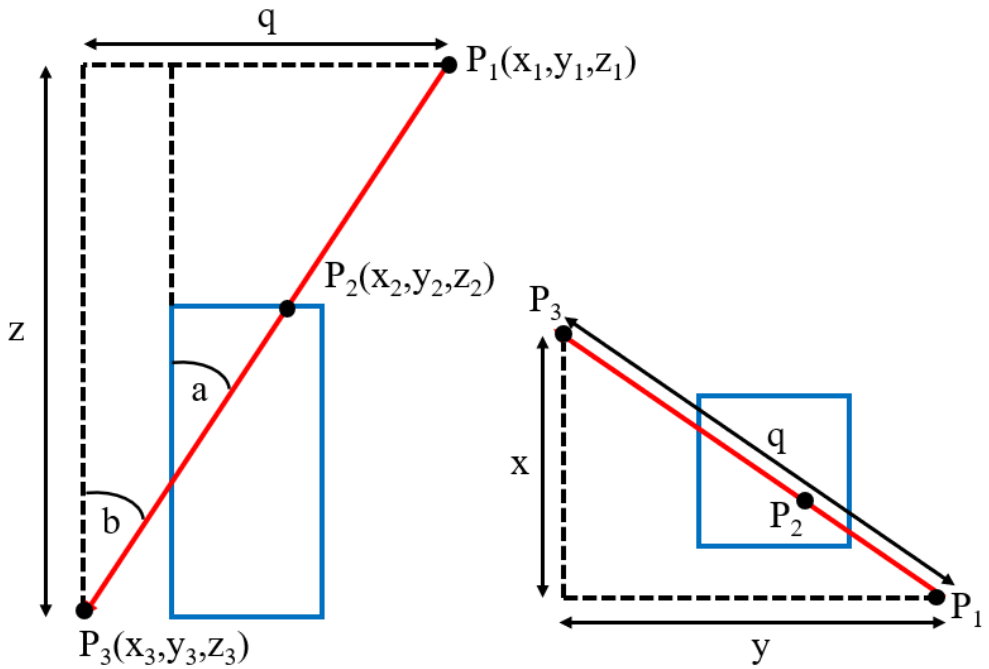

Figure 10: Schematic of the geometry of a single particulate track and associated scattering angles. Left – A side profile is shown of the particulate track entering the micropore. Right – A birds-eye view of the same schematic, highlighting key dimensions in calculating the scattering angle b.

Substituting Eq. 2 into Eq. 3 leads to the following expression which describes the incident angle in which a particulate strikes the inner wall of the micropore:

$$b = \tan^{-1}\left[\frac{\sqrt{(x^2+y^2)}}{z}\right] \qquad \text{Eq. 4}$$

Using Eq. 4 it is possible to calculate the crucial incident particulate angle, which when evaluated against the critical angle of scattering, provides the information as to whether a particulate scatters off the inner surface of the micropore and exits successfully. Figure 11 below shows the distribution of calculated incident angles for differing pore ratios.

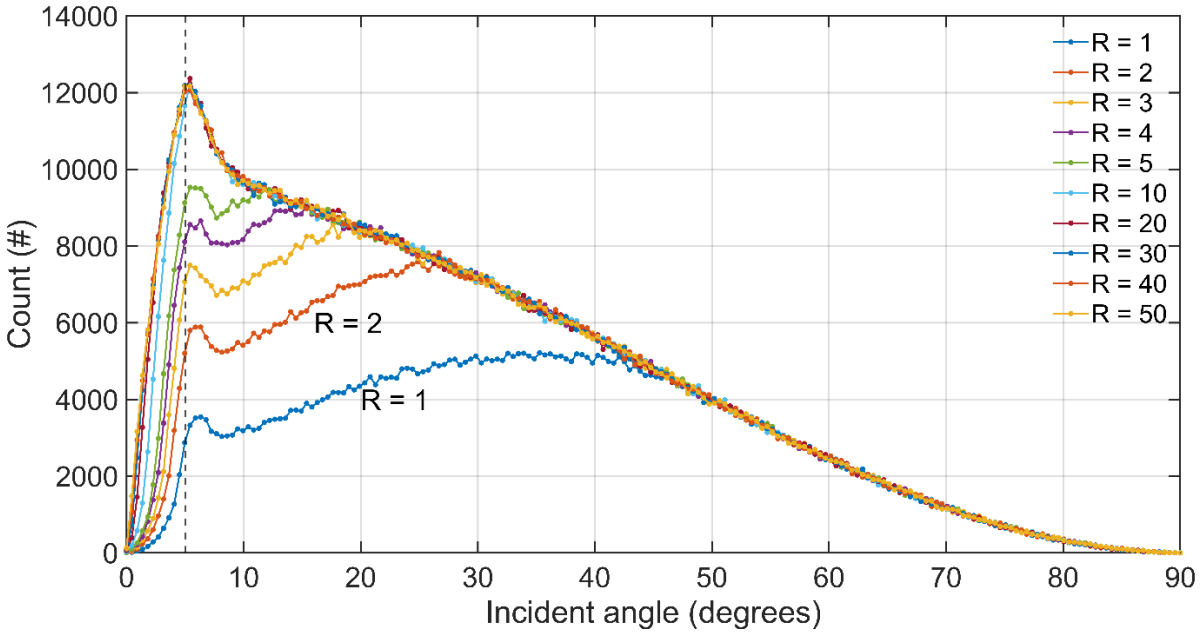

Figure 11: Angular distribution for differing pore ratios, where the incident angle is measured from the normal to the plane of the entrance of the micropore.

For angles above 45 degrees, regardless of pore ratio, the relationship between count and scattering angle is identical, with a gradual decrease in count with respect to increasing incident angle. Considering the initial generation of points followed an angular cosine distribution, the gradual decrease in count after 45 degrees is consistent with the tail of a cosine distribution. Below 45 degrees however, the angular distribution is not consistent across different pore ratios. A distinct cut-off point exists for each pore ratio, where below this angular cut-off, the distribution changes, often exhibiting the opposite behaviour as is seen above 45 degrees. As pore ratio increases, this cut-off point decreases until the pore ratio approaches the values of ~ 5-10. At this point, and for pore ratios above, the angular distribution is identical.

For pore ratio above 10, a sharp peak in seen at ~ 5 degrees followed by a sharp decrease in count for the next 5 degrees. After 10 degrees however, the gradient is still negative but decreases at a slower rate. The exact reason for this peak location is unknown at this stage, however smaller peaks are also seen in higher pore ratios. For pore ratios below 10, the overall count decreases, especially at lower angles (below 45 degrees). The physical explanation for this may be due to the combination of low pore ratio and low incident angle increasing the number of directly transmitted particulates, although it is hard to explicitly confirm this with Figure 11 above.

4.9 Ratio of direct and non-direct transmission versus pore ratio

Once the number of directly and non-directly transmitted particulates are calculated, the total transmission rate can be calculated for different pore ratios. Figure 12 shows the number of transmitted particulates plotted as a function of both pore ratio and percentage of total incident particulates. Also shown is the overall transmission rate for comparison.

At low pore ratios, the transmission rate is at a maximum, which is dominated by particulates which are directly transmitted through the pore. As pore ratio increases, both the percentage of particulates directly transmitted decreases along with overall transmission rate. This suggests that for low pore ratios, the transmission rate is dominated by directly transmitted particulates. Above a pore ratio of ~10, a steady state is reached, with transmission rate now dominated by scattered particulates and the number of particulates directly transmitted is negligible. Physically, this is intuitive as the micropores are now significantly longer than the entrance dimensions, so the chance of a particulate traversing the entire length of a micropore without scattering is small. Furthermore, the result seen in Figure 12 is also consistent with the result in Figure 11, as after the pore ratio goes above ~10, a steady state is seen, with regards to both transmission rate and the angular distributions.

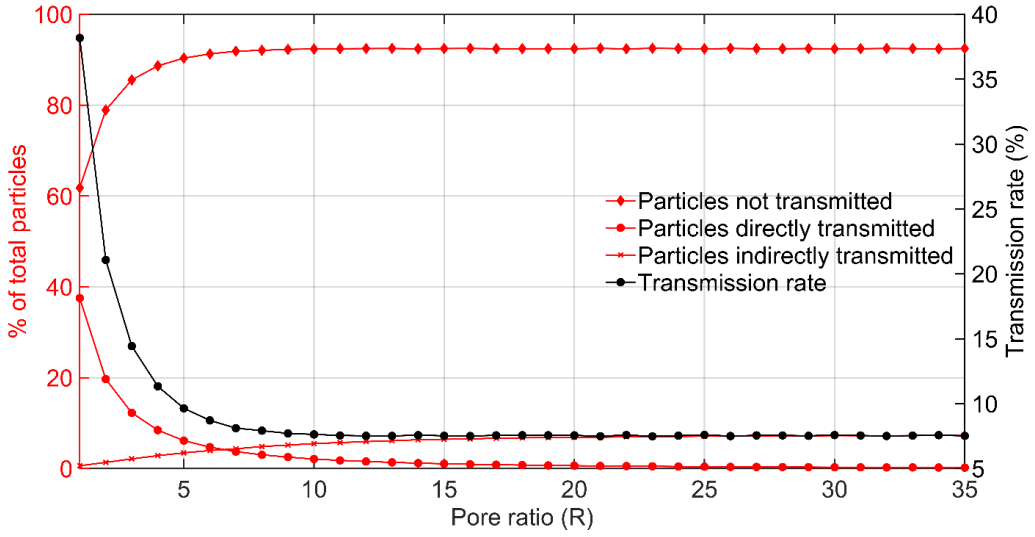

Figure 12: Proportion of total particulates that are either not transmitted, transmitted indirectly or transmitted directly through a single micropore as a function of pore ratio. The particulate diameter used for these simulations was $1x10^{-6}$ m, with a square pore diameter of $40x10^{-6}$ m.

4.10 Overall particulate transmission rates

By using Eq. 1, it is possible to calculate the overall transmission rate of particulates through an example micropore. Figure 13 shows the transmission rate (as a percentage of particulates incident) as a function of particulate diameter for a range of different pore ratios. In this example a 40 µm square pore width is used. The trends shown in Figure 13 are consistent with the physics incorporated within the Monte Carlo simulation. For example, particulate transmission rates rapidly decrease towards a 40 µm particulate diameter (for all pore ratios), which is equal to the simulated micropore entrance size. This shows that the EPA reduction is working as intended, and particulates that are larger than the entrance to the micropore cannot enter the pore and hence are not transmitted. Furthermore, transmission rates are generally lower as pore ratio is increased. Thinner and longer pores are simply more difficult to traverse for particulates and this is shown by the model.

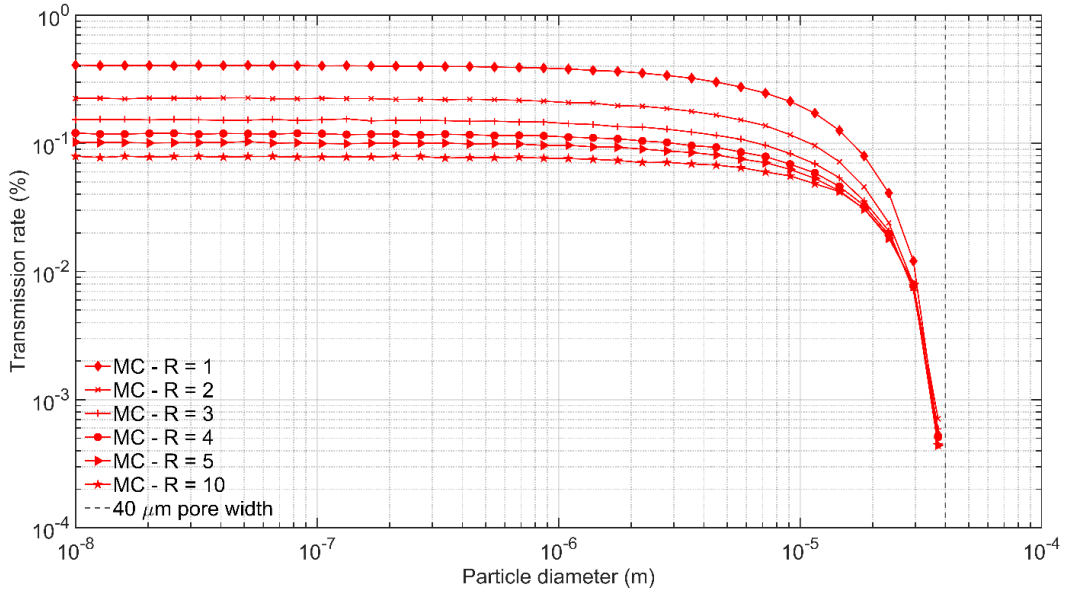

Figure 13: Overall particulate transmission rate values produced by the Monte Carlo simulation for differing pore ratios. R values of 20, 30, 40 were computed but the transmission rates were identical to those of R = 10, so they were omitted for clarity.

5 Conclusions and future work

A bespoke Monte Carlo simulation was developed, based upon previous particulate scattering mechanisms observed in nested mirror, soft X-ray optics. The simulation was described from first principles, with each stage of the methodology explained. The simulation produces physical, intuitive results for different pore ratios and simulated particulate diameters. For micropore R values of R > 10 (such as the SMILE and THESEUS micropore sizes), the approximate transmission rate is 0.1% for particles below 1 micron diameter, with the transmission rate of larger particles rapidly decreasing for particles larger than 1 micron in diameter.

The work contained here can benefit greatly from an experimental campaign, focusing on scattering mechanisms within sMPO. The author has built and assembled a vacuum chamber capable of holding a CCD270, which can be interfaced with a Van De Graaf generator, providing the accelerating mechanism required for a hyper-velocity particulate impacts campaign. The campaign is part of a distinct work package as part of the ESA mission SMILE and will commence in the coming months. Results produced from the experimental campaign will allow the transmission rates predicted here to be explicitly compared.

The work contained in this paper can be beneficial to any space mission utilising the next generation of soft X-ray optics (sMPO). It can be combined with known flux models and damage equations to, for the first time, quantify the risk of hyper-velocity particulate impacts to the focal planes of large-scale space missions.

6 References

[1] Strüder, L., Briel, U., Dennerl, K., et al. 2001, A&A, 365, L18

[2] Weisskopf M. C. Brinkman B. Canizares C. Garmire G. Murray S. Van Speybroeck L. P.2002, PASP, 114, 1

[3] Bavdaz, M, et al, “Silicon Pore Optics developments and status”, Proc. of SPIE 8443, 844329(2012)

[4] Norbert Meidinger, Bernd Aschenbach, Heinrich W Braeuninger, Gerhard Drolshagen, Jakob Englhauser, Robert Hartmann, Gisela D Hartner, Ralf Srama, Lothar Strueder, Martin Stuebig, et al. Experimental verification of a micrometeoroid damage in the pn-ccd camera system aboard xmm-newton. In Astronomical Telescopes and Instrumentation, pages 243–254. International Society for Optics and Photonics, 2003.

[5] A.F. Abbey, R.M. Ambrosi, and A. Wells “Effects of micrometeoroid and space debris impacts in grazing incidence telescopes”, Proc. SPIE 6266, Space Telescopes and Instrumentation: Ultraviolet to Gamma Ray, 62663K (15th June 2006); https://doi.org/10.1117/12.677410

[6] Palmieri, D. 2004, ESA report EWP-2167

[7] Santin, G., “Normalization modelling sources,” Slides, 4-8 June 2007, < http://geant4.in2p3.fr/2007/prog/GiovanniSantin/GSantin_Geant4_Paris07_Normalisation_v07.pdf> (2 November 2020).

[8] Soman, M. R., Hall, D. J., Holland, A. D., Burgon, R., Buggey, T., Skottfelt, J., Sembay, S., Drumm, P., Thornhill, J., Read, A., Sykes, J., Walton, D., Branduardi-Raymont, G., Kennedy, T., Raab, W., Verhoeve, P., Agnonol, D., & Woffinden, C. (2018). *The SMILE Soft X-ray Imager (SXI) CCD design and development.* Journal of Instrumentation, 13(1), article no. C01022.

[9] Photonis. (2020). *Photonis*. [online] Available at:https://www.photonis.com/products/micro-pore-optics.